JACS
JOURNAL OF THE AMERICAN CHEMICAL SOCIETY
pubs.acs.org/JACS
Article

Iodine−Iodine Cooperation Enables Metal-Free C−N Bond-Forming Electrocatalysis via Isolable Iodanyl Radicals

Brandon L. Frey, Matthew T. Figgins, Gerard P. Van Trieste, III, Raanan Carmieli, and David C. Powers*

Cite This: J. Am. Chem. Soc. 2022, 144, 13913−13919
Read Online
ACCESS | Metrics & More | Article Recommendations | Supporting Information

ABSTRACT: Small molecule redox mediators convey interfacial electron transfer events into bulk solution and can enable diverse substrate activation mechanisms in synthetic electrocatalysis. Here, we report that 1,2-diiodo-4,5-dimethoxybenzene is an efficient electrocatalyst for C−H/E−H coupling that operates at as low as 0.5 mol % catalyst loading. Spectroscopic, crystallographic, and computational results indicate a critical role for a three-electron I−I bonding interaction in stabilizing an iodanyl radical intermediate (*i.e.*, formally I(II) species). As a result, the optimized catalyst operates at more than 100 mV lower potential than the related monoiodide catalyst 4-iodoanisole, which results in improved product yield, higher Faradaic efficiency, and expanded substrate scope. The isolated iodanyl radical is chemically competent in C−N bond formation. These results represent the first examples of substrate functionalization at a well-defined I(II) derivative and *bona fide* iodanyl radical catalysis and demonstrate one-electron pathways as a mechanistic alternative to canonical two-electron hypervalent iodine mechanisms. The observation establishes I−I redox cooperation as a new design concept for the development of metal-free redox mediators.

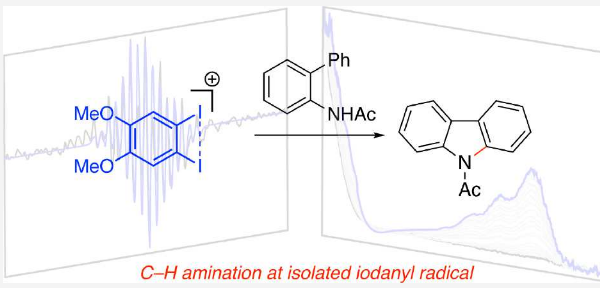

■ INTRODUCTION

The development of indirect electrochemical mediators, which are redox-active small molecules that participate in well-defined interfacial electron transfer (ET) and convey the resulting electron or hole equivalents into the bulk phase, has powerfully enabled the development of organic electrocatalysis.[1,2] Identification of new mediators that engage in diverse modes of substrate activation and that can aggregate the multiple electron equivalents needed for the two-electron bond-making processes in organic synthesis provides the opportunity to marry interfacial electron transfer with an array of synthetic transformations. Hypervalent iodine compounds are a broadly deployed class of chemoselective oxidants,[3−7] and the potential to utilize aryl iodides as indirect electrochemical mediators (*i.e.*, electrocatalysts) has garnered significant attention (Figure 1).[8−12] Thus far, high catalyst loading, limited substrate scope, and the high onset potential for anodic oxidation has stymied the development of hypervalent iodine electrocatalysis and largely limited application of these mediators to *ex cell* transformations.[13,14]

Organic hypervalent I(III) and I(V) reagents are commonly encountered oxidants in fine-chemical synthesis that operate via selective two-electron oxidation−reduction processes. The potential role of iodanyl radicals (*i.e.*, formally I(II) species) in substrate functionalization chemistry is far less explored.[15−17] Recently, transient iodanyl radicals have been proposed as intermediates in the photochemistry of I(III) compounds[18] and as intermediates in aerobic and electrochemical syntheses

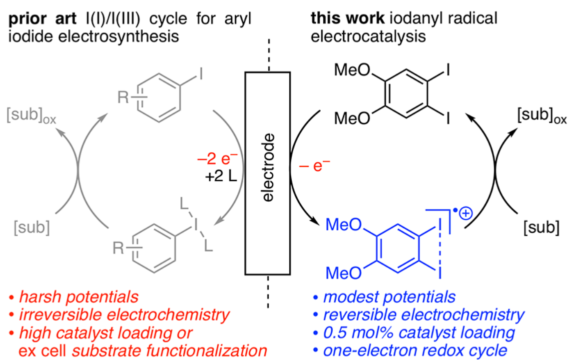

Figure 1. Strategies for hypervalent iodine electrochemistry, either multiple-electron oxidation to form I(III) species or single-electron oxidation for iodanyl radical electrocatalysis.

of I(III) derivatives.[11,18−20] For example, in 2020, we reported an electrochemical C−H/N−H coupling catalyzed by iodoanisole that was proposed to proceed via carboxylate-stabilized iodanyl radicals.[11] While increasingly invoked, the

Received: May 25, 2022
Published: July 20, 2022

https://doi.org/10.1021/jacs.2c05562
J. Am. Chem. Soc. 2022, 144, 13913−13919

complete lack of isolable organic I(II) compounds has prevented interrogation of potential reactions of these open-shell species toward substrates.

Inspired by (1) the reversible electrochemistry of veratrole derivatives (*i.e.*, dimethoxybenzenes)[21] and (2) the delocalized I−I interactions in σ-aromatic $C_6I_6^{2+}$,[22] we identified 1,2-diiodo-4,5-dimethoxybenzene (**1a**) as a highly efficient and robust catalyst for a suite of C-H functionalization reactions at catalyst loadings as low as 0.5 mol %. Detailed electrochemical and *in situ* spectroscopic experiments indicate that these reactions are mediated by the iodanyl radical generated by one-electron oxidation of **1a**. Synthesis and isolation of the iodanyl radical ($\mathbf{1a}^+$) enabled complete spectroscopic and crystallographic characterization. The isolated iodanyl radical is chemically competent as an intermediate in C−H functionalization. These observations raise the specter of I(I/II) catalytic cycle involving direct substrate engagement by an iodanyl radical, which contrasts with traditional two-electron hypervalent iodine cycles.

■ EXPERIMENTAL SECTION

Representative procedures are presented below; for detailed descriptions of materials, methods, synthetic procedures for starting materials, and characterization data, see the Supporting Information.

Synthesis of 1,2-Diiodo-4,5-Dimethoxybenzene Radical Cation ($\mathbf{1a}^+$). A 100-mL round bottom flask was charged with **1a** (184 mg, 0.472 mmol, 1.00 equiv), bis(trifluoroacetoxy)iodobenzene (PIFA) (104 mg, 0.242 mmol, 0.513 equiv), and CH_2Cl_2 (10 mL). The reaction mixture was cooled to −20 °C. $BF_3{\cdot}OEt_2$ (60.0 μL, 0.486 mmol, 1.03 equiv) was added dropwise, resulting in an immediate blue color and further stirred at −20 °C for 3 h. The reaction was then filtered through a fine frit, washed with cold CH_2Cl_2, and dried under reduced pressure to afford $\mathbf{1a}^+$ (121 mg, 55% yield) as a dark blue solid. UV−vis spectroscopy: λ_{max} = 613 nm in hfip. Single crystals were obtained from the blue concentrated filtrate upon standing at −20 °C for 16 h; data are summarized in Figure 4a and Tables S4, S6, and S7.

Reaction of $\mathbf{1a}^+$ with 2. A 20 mL scintillation vial was charged with $\mathbf{1a}^+$ (95.4 mg, 0.201 mmol, 2.00 equiv) and **2** (21.2 mg, 0.100 mmol, 1.00 equiv) in hfip (5.0 mL). The reaction mixture was cooled to 0 °C. Tetramethylammonium acetate (26.6 mg, 0.187 mmol, 0.929 equiv) was added batchwise at 0 °C before the reaction was allowed to warm to 23 °C and stirred for an additional 6 h. The reaction was then concentrated under reduced pressure and diluted with $CDCl_3$, and trimethoxybenzene (10.0 mg, 0.60 mmol) was added as an internal standard. The reaction outcome was analyzed by ^{1}H NMR spectroscopy to show product **3** (35% yield) and **1a** (quant.). Compound **3**: ^{1}H NMR (δ, 23 °C, 400 MHz, $CDCl_3$): 7.38 (d, *J* = 8.8 Hz, 2H), 6.91 (d, *J* = 8.8 Hz, 2H), 5.85 (s, 1H), 4.22 (td, *J* = 9.8, 4.5 Hz, 1H), 4.16−4.09 (m, 2H), 3.81 (s, 3H), 2.18 (s, 3H). The obtained spectral data were in good agreement with the literature.[11]

Intramolecular C−N Coupling Catalyzed by 1a. A 10 mL glass vial was charged with *N*-arylacetamide **2** (42.4 mg, 0.201 mmol, 1.00 equiv), **1a** (1.00×10^{-3} mmol, 0.5 mol %), tetramethylammonium acetate (57.0 mg, 0.401 mmol, 1.99 equiv), tetrabutylammonium hexafluorophosphate (390 mg, 1.01 mmol, 5.02 equiv), and hfip (5.0 mL) and was fitted with a glassy carbon anode, platinum cathode, and Ag^+/Ag reference electrode. Constant potential electrolysis was applied to the reaction mixture at 1.22 V vs Fc^+/Fc, until ∼50 C charge (∼2.6 F/mol) was passed. The reaction was then concentrated under reduced pressure and diluted with $CDCl_3$; trimethoxybenzene (10.0 mg, 0.60 mmol) was added as an internal standard; and the reaction outcome was analyzed by ^{1}H NMR spectroscopy to show product **3** (92% yield). Spectral data are consistent with those reported above.

Spirocyclization of 4 Catalyzed by 1a. A 10 mL glass vial was charged with **4** (47.7 mg, 0.201 mmol, 1.00 equiv), **1a** (2.01×10^{-3} mmol, 1 mol %), tetramethylammonium acetate (57.0 mg, 0.401 mmol, 1.99 equiv), tetrabutylammonium hexafluorophosphate (390 mg, 1.01 mmol, 5.02 equiv), and hfip (5.0 mL) and was fitted with a glassy carbon anode, platinum cathode, and Ag^+/Ag reference electrode. Constant potential electrolysis was applied to the reaction mixture at 1.22 V vs Fc^+/Fc, until ∼50 C charge (∼2.6 F/mol) was passed. The reaction was then concentrated under reduced pressure and diluted with $CDCl_3$; trimethoxybenzene (10.0 mg, 0.60 mmol) was added as an internal standard; and the reaction outcome was analyzed by ^{1}H NMR spectroscopy to show product **5** (61% yield). ^{1}H NMR (δ, 23 °C, 400 MHz, $CDCl_3$): 6.94 (d, *J* = 10.2 Hz, 2H), 6.37 (d, *J* = 10.1 Hz, 2H), 6.14 (s, 1H), 2.70 (t, *J* = 7.9 Hz, 2H), 2.38 (t, *J* = 8.0 Hz, 2H), 2.14 (s, 2H). The obtained spectral data were in good agreement with the literature.[20]

Lactonization of 6 Catalyzed by 1a. A 10 mL glass vial was charged with **6** (39.8 mg, 0.201 mmol, 1.00 equiv), **1a** (0.101 mmol, 5 mol %), tetramethylammonium acetate (57.0 mg, 0.401 mmol, 1.99 equiv), tetrabutylammonium hexafluorophosphate (390 mg, 1.01 mmol, 5.02 equiv), and hfip (5.0 mL) and was fitted with a glassy carbon anode, platinum cathode, and Ag^+/Ag reference electrode. Constant potential electrolysis was applied to the reaction mixture at 1.22 V vs Fc^+/Fc, until ∼50 C charge (∼2.6 F/mol). The reaction was then concentrated under reduced pressure and diluted with $CDCl_3$; trimethoxybenzene (10.0 mg, 0.60 mmol) was added as an internal standard; and the reaction outcome was analyzed by ^{1}H NMR spectroscopy to show product **7** (99% yield). ^{1}H NMR (δ, 23 °C, 400 MHz, $CDCl_3$): 8.38 (dd, *J* = 8.2, 1.2 Hz, 1H), 8.21 (d, *J* = 7.9 Hz, 1H), 8.15 (dd, *J* = 8.1, 1.4 Hz, 1H), 7.92 (td, *J* = 7.8, 1.3 Hz, 1H), 7.67−7.63 (m, 1H), 7.58−7.53 (m, 1H), 7.45−7.36 (m, 4H). The obtained spectral data were in good agreement with the literature.[23]

Benzylic Acetoxylation of 8 Catalyzed by 1a. A 10 mL glass vial was charged with **8** (39.0 mg, 0.201 mmol, 1.00 equiv), **1a** (19.5 mg, 0.0500 mmol, 25 mol %), tetramethylammonium acetate (57.0 mg, 0.401 mmol, 1.99 equiv), tetrabutylammonium hexafluorophosphate (390 mg, 1.01 mmol, 5.02 equiv), and hfip (5.0 mL) and was fitted with a glassy carbon anode, platinum cathode, and Ag^+/Ag reference electrode. Constant potential electrolysis was applied to the reaction mixture at 1.22 V vs Fc^+/Fc, until ∼50 C charge (∼2.6 F/mol). The reaction was then concentrated under reduced pressure and diluted with $CDCl_3$; trimethoxybenzene (10.0 mg, 0.60 mmol) was added as an internal standard; and the reaction outcome was analyzed by ^{1}H NMR spectroscopy to show product **9** (74% yield). ^{1}H NMR (δ, 23 °C, 400 MHz, $CDCl_3$): 7.38 (d, *J* = 8.8 Hz, 2H), 6.91 (d, *J* = 8.8 Hz, 2H), 5.85 (s, 1H), 4.22 (dq, *J* = 9.8, 4.5 Hz, 1H), 4.16−4.09 (dq, *J* = 9.8, 4.5 Hz, 1H), 3.81 (s, 3H), 2.18 (s, 3H), 1.24 (t, 7.13 Hz, 3H). ^{13}C NMR (δ, 23 °C, 400 MHz, $CDCl_3$): 170.4, 169.1, 160.3, 129.1, 126.0, 114.2, 74.3, 61.6, 55.3, 20.8, 14.0. HRMS−ESI: calculated for [M + Na] = 175.0890, observed [M + Na] = 175.0884.

■ RESULTS AND DISCUSSION

We initiated our studies by examining the impact of aryliodide structure on the electrochemical C−N coupling of biarylamide **2** to afford the corresponding carbazole (**3**). Previous attempts to lower the catalyst loading from 25 mol % (optimized condition with 4-iodoanisole (**1b**) as catalyst) resulted in a significantly decreased reaction efficiency: At 5 mol % **1b**, only 30% carbazole was produced and lowering further to a 0.5 mol % catalyst loading resulted in 6% carbazole formation (Figure 2a, Table S1). 4-Iodo-1,2-dimethoxybenzene (**1c**), which features a second methoxy substituent, displayed significantly increased electrochemical reversibility and decreased the onset potential for oxidation but showed poor catalytic activity (8% yield in cyclization of **2**). 1,2-Diiodo-4-methoxybenzene (**1d**), which features a second iodine substituent, displays poorer electrochemical reversibility and neither lowered the observed $E_{1/2}$ nor resulted in improved catalysis. In contrast, 1,2-diiodo-

https://doi.org/10.1021/jacs.2c05562
J. Am. Chem. Soc. 2022, 144, 13913−13919

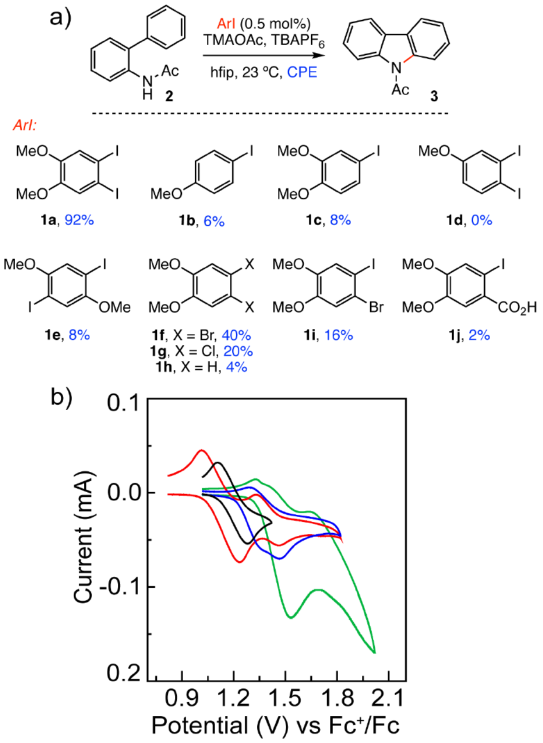

Figure 2. (a) Impact of catalyst structure on cyclization efficiency. Conditions: CPE at the E_{pa} of **1** determined by CV in an undivided cell with a glassy carbon anode, a platinum-plated cathode, and a Ag^{+}/Ag reference electrode. (b) CVs of **1a** (black line), **1b** (blue line), **1c** (red line), and **1d** (green line) measured using **1** (5 mM) in 0.2 M $TBAPF_6$/hfip at 0.1 V/s.

4,5-dimethoxybenzene (**1a**), which features two iodine and two methoxy substituents, displays a reversible wave at $E_{1/2}$ = 1.13 V vs Fc^{+}/Fc and a 200 mV lower E_{pa} than **1b** (Figure 2b) and is a highly efficient catalyst. With **1a**, the catalyst loading could be lowered to 0.5 mol % with no loss of yield or FE (*i.e.*, 92% yield, 73% FE, Figure 2a).

The relative position of the iodine substituents is crucial to catalytic efficiency: 1,4-diiodo-2,5-dimethoxybenzene (**1e**) displays $E_{1/2}$ = 1.09 V vs Fc^{+}/Fc but is an inefficient C−N coupling catalyst (8% yield in cyclization of **2**). Other 1,2-dimethoxybenzene derivatives were evaluated including 1,2-dibromo-4,5-dimethoxybenzene (**1f**), 1,2-dichloro-4,5-dimethoxybenzene (**1g**), and 1,2-dimethoxybenzene (**1h**). At a 0.5 mol % catalyst loading, these aryl iodides afforded carbazole **3** in 40, 20, and 4% yields, respectively (Figure 2a). The mixed halogen catalyst 1-bromo-2-iodo-4,5-dimethoxybenzene (**1i**) performed worse compared to the dihalides **1a**, **1f**, or **1g** affording **3** in 16% yield. Finally, we also examined 2-iodo-4,5-dimethoxybenzoic acid (**1j**) based on previous proposals that carboxylate ligands can stabilize iodanyl radicals generated from the reduction of I(III) reagents.[24,25] At a 0.5 mol % catalyst loading, **1j** afforded only a 2% yield of **3**. Additional electron-rich aryl iodides were examined and were generally poorly efficient catalysts (Figure S1).

The nature of the electrochemical processes observed of **1a** was analyzed by examining the relative cathodic (I_{PC}) and anodic currents (I_{PA}) as well as the separation of the oxidation and reduction peaks (ΔE_p) in CVs of **1a**. In these experiments, CVs were obtained for hfip solutions of **1a** with [TBA]PF_6 as the electrolyte and a scan rate of 0.1 V/s. Under these conditions, the I_{pc}/I_{pa} ratio, which provides a measure of electrochemical reversibility and thus the stability of the electrochemically generated species, was 0.94 (*c.f.* under these conditions, I_{pa}/I_{pc} = 1.0 for ferrocene; Figure 3a). ΔE_p for **1a** was measured to be 183 mV; for comparison, ΔE_p for ferrocene was 187 mV under these conditions (Figure 3a). The significant deviation from ideality (*i.e.*, ΔE_p = 59 mV) likely results from slow electron transfer kinetics under the reaction conditions.[26,27] Analogous results were obtained at different scan rates (Figure S2 and Table S2). Further support for a one-electron event was obtained by integration of the square-wave voltammetry data of **1a** and Fc, which display similar areas (Figure 3b and Figure S3).[28] Analyses of other veratrole derivatives showed significantly less electrochemical reversibility, which we speculate may result in poor catalyst performance (Figure S4 and Table S3).

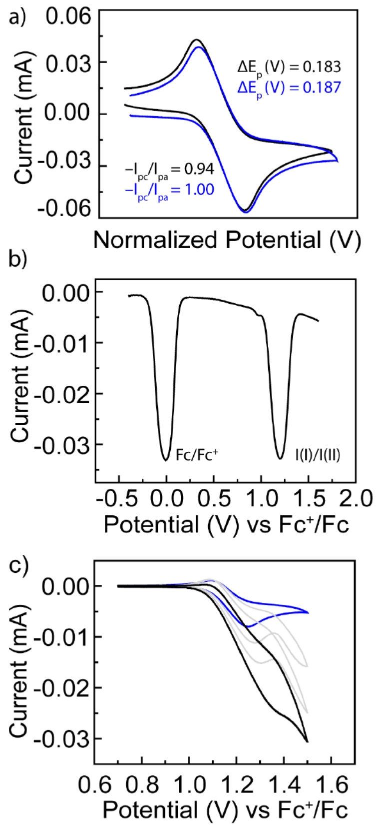

Figure 3. (a) Cyclic voltammograms of 5.0 mM **1a** in a 0.2 M $TBAPF_6$/hfip solution (black line) and 5.0 mM ferrocene in a 0.2 M $TBAPF_6$/hfip solution (blue line) at 0.1 V/s with normalized potentials. (b) Square wave voltammetry of a 5.0 mM **1a** and 0.5 mM ferrocene in a 0.2 M $TBAPF_6$/hfip solution. (c) CVs of **1a** (5 mM) with 35.5 mM [TMA]OAc in 0.2 M $TBAPF_6$/hfip at 0.1 V/s varying biarylamide **2** loadings at 0 (blue line), 1.9, 6.1, and 12 mM (black line).

To gain insight into the impact of substrate (**2**) and acetate, which is required for efficient C−N coupling, CVs were measured as a function of the concentration of these species. Addition of [TMA]OAc to CV solutions of **1a** resulted in increased oxidative current and partial loss of reversibility (Figure S5, I_{pc}/I_{pa} = 0.52 with 35.5 mM [TMA]OAc). We previously interpreted similar observations in CVs of 4-iodoanisole **1b** as consistent with acetate binding to an anodically generated iodanyl radical.[11] In the case of **1a**, reversibility can be recaptured at higher scan rates (Figure S6). Addition of substrate **2** to CVs of **1a** does not affect the reversible wave observed for **1a** (a new peak at E_{pa} = 1.55 V vs Fc^+/Fc grows in Figure S7, a result of direct substrate oxidation (Figure S8)). Addition of both **2** and [TMA]OAc to CVs of **1a** resulted in the observation of catalytic current where reversibility could not be regained regardless of the scan rate, indicative of rapid catalytic turnover (Figure 3c).

Given the single-electron inventory indicated by CV analysis, we were interested in the possibility that substrate activation may arise from one-electron oxidation of **1a** without subsequent generation of an I(III) intermediate. Constant potential electrolysis (CPE) of an hfip solution of **1a** (0.2 M [TBA]PF_6 added as electrolyte) in the absence of either acetate or **2** resulted in a drastic color change from colorless to dark blue (Figure 4). The UV–vis spectrum of this solution, acquired *in situ* via spectroelectrochemistry or *ex situ* following the cessation of electrolysis, displayed a broad low-energy absorbance centered at 613 nm (Figure 4a (black line) and Figures S9 and S10). Acquisition of spectra periodically during the electrolysis reveals the presence of an isosbestic point at 380 nm, which indicates the lack of a steady state intermediate in the anodic oxidation of **1a**. The observed UV–vis spectrum is consistent with reported veratrole-derived radical cations[21,29,30] (red shifted due to the heavy atom effect of two iodides). Time-dependent density functional theory (TD-DFT) computations reproduce the low-energy feature in the spectrum of **1a**$^+$ (λ_{max} = 645 nm, Figure 4a (blue line and red line)).[31] The largest orbital contribution to this transition is β-HOMO(−2) to β-LUMO, which is primarily π-to-π^* with significant contribution from the in-phase combination of I-centered p-orbitals (Figure 4b).

Two experiments were carried out to confirm that the blue solution represented single-electron oxidation of **1a**. First, the addition of one equivalent of *N,N*-dimethylaniline results in the consumption **1a**$^+$ (with concurrent regeneration of **1a**) and the quantitative evolution of the *N,N*-dimethylaniline radical cation (Figure S11). Second, *in situ* EPR experiments[32] are consistent with one-electron oxidation of **1a** to generate an open-shell species. The resulting spectrum displays a narrow spectral width (25 G) that is well-simulated with $2a_I$ = 1.67 G, $2a_H$ = 3.35 G, and $2a_{Me}$ = 0.343 G (Figure 4c). For comparison, under identical *in situ* conditions, neither 4-iodotoluene nor 4-bromoanisole provides a spectral signature (Figure S12).

To simplify isolation and independent characterization of iodanyl radical **1a**$^+$, we pursued chemical oxidation of **1a** to avoid the use of supporting electrolyte. Inspired by Kita's seminal work on single-electron oxidation of anisole derivatives by bis(trifluoroacetoxy)iodobenzene (PIFA),[33,34] we found that treatment of **1a** with 0.5 equivalents of bis-(trifluoroacetoxy)iodobenzene (PIFA) and excess $BF_3{\cdot}OEt_2$ in CH_2Cl_2 resulted in a dark-blue solution that was spectroscopically identical to the electrochemically generated solution (for comparison of UV–vis spectra and solvatochromism, see Figure S13).[35] Dark blue X-ray quality single-crystals of **1a**$^+$ were obtained on prolonged standing of reaction solutions at −22 °C (Figure 5a; solid-state and solution-phase

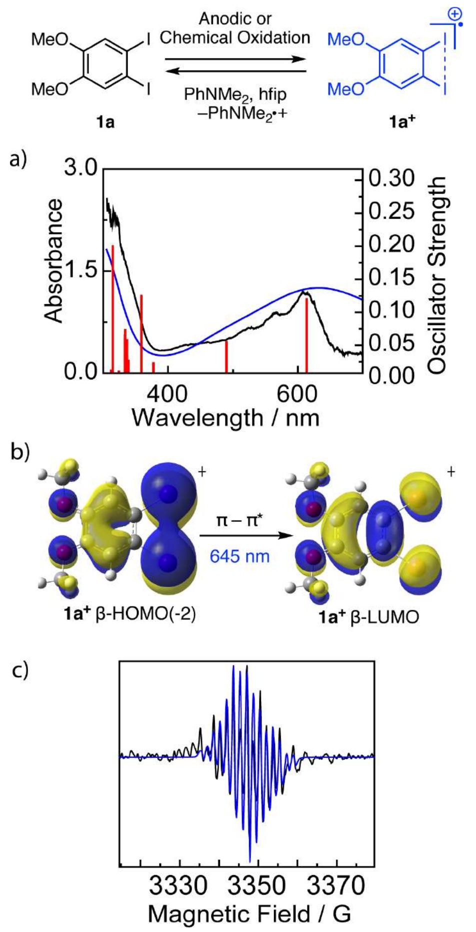

Figure 4. Oxidation of **1a** affords iodanyl radical **1a**$^+$. Oxidation: 5 mM **1a** in a 0.2 M TBAPF_6/hfip solution, CPE 1.22 V vs Fc^+/Fc; or, 0.5 equivalents PIFA, $BF_3{\cdot}OEt_2$ in CH_2Cl_2. Reduction: 1.0 equivalent of *N,N*-dimethylaniline in hfip. (a) *In situ* UV–vis spectra collected during CPE of 5 mM **1a** (black line). TD–DFT absorption spectrum of **1a**$^+$ (blue line) and electronic configurations of excited states for **1a**$^+$ (red line). (b) Most significant contributors to the computed transition at 645 nm. (c) *In situ* EPR spectra collected during a CPE of 1 mM **1a** (black line) and simulated spectrum of **1a**$^+$ (blue line).

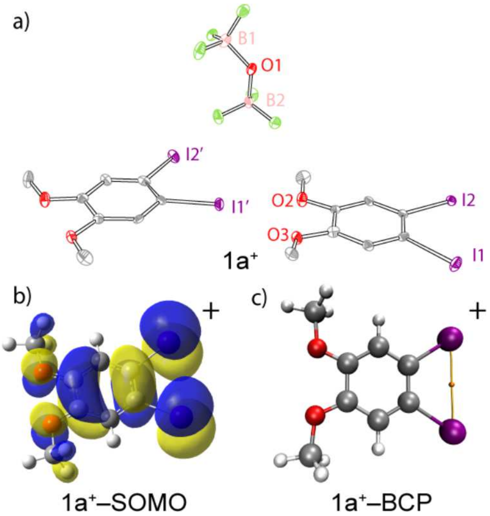

Figure 5. (a) Displacement ellipsoid plot of **1a**$^+$ drawn at 50% probability, H-atoms are omitted for clarity. Selected metrical parameters: C1−I1 = 2.076(6) Å, I1−I2 = 3.6392(7) Å, B1−O1 = 1.513(9) Å, B2−O1 = 1.520(9) Å. (b) Computed SOMO of **1a**$^+$. (c) Atoms-in-molecules (AIM) analysis indicates an I−I bond critical point (BCP).

https://doi.org/10.1021/jacs.2c05562
J. Am. Chem. Soc. 2022, 144, 13913−13919

UV−vis of redissolved crystals are collected in Figure S13). X-ray diffraction of the obtained single crystals provided the molecular structure shown in Figure 4a. The metrical parameters of **1a** are similar to those of **1a**$^+$, with the exception of a marked contraction of the I−I distance from 3.71157(2) in **1a** to 3.6391(7) in **1a**$^+$ (for complete comparison of **1a** and **1a**$^+$, see Figure S14 and Tables S4−S6). Charge balance in the crystal is maintained by 0.5 $B_2F_6O^{2-}$ dianions per **1a**$^+$(see Table S7 and Figure S15 for refinement details).

Oxidation of **1e**-**1j** under the same conditions used for the preparation of **1a**$^+$ resulted in significant and distinct color changes. Oxidation of compounds **1f** and **1g** produced red and yellow solutions, respectively (Figure S16a). Oxidation of **1e**, **1i**, and **1j** afforded purple solutions; in the case of **1j**, the color dissipated quickly, which may be due to decarboxylative decomposition (Figure S16b). Treatment of veratrole (**1h**) under these conditions did not result in an observed color change. Unfortunately, attempts to crystalize these radical cations (*i.e.,* **1e**$^+$-**1j**$^+$) were unsuccessful.

DFT optimized structures of **1a** and **1a**$^+$ provide metrics that are in close agreement with those determined by X-ray crystallography (Tables S8 and S9). In particular, the noted contraction of the I−I vector is well described in the computed structures: one-electron oxidation leads to a computed I−I contraction from 3.70 Å for **1a** to 3.65 Å for **1a**$^+$. The singly occupied molecular orbital (SOMO) of **1a**$^+$ displays a predominantly π-character with significant orbital contribution from the iodine atoms (~35% iodine-iodine AO contribution to the SOMO, Figure 5b). We envisioned that the observed I−I contraction may arise from oxidatively induced delocalized 3-electron bonding, which is well-precedented in proximal heavy main-group elements, such as diselenides and disulfides[36−38] but unknown in hypervalent iodine chemistry. Atoms-in-molecules (AIM) analysis indicates an electron density of ρ(r) = 0.0123 e·bohr^{-3} and a Laplacian distribution of $\nabla^2\rho$(r) = 0.0323 e·bohr^{-5} at the I−I bond critical point (BCP) for **1a**$^+$ (Figure 5c). For comparison, no BCP is observed between the I atoms in **1a** (Figure S17). The ρ(r) observed at the BCP of **1a**$^+$ is within the range of values expected for I−I bonds.[39]

AIM analysis was also carried out for **1f**$^+$, **1g**$^+$, **1i**$^+$, and **1j**$^+$. No BCPs were observed for radical cations derived from the *ortho*-dibromo (*i.e.,* **1f**$^+$), *ortho*-dichloro (*i.e.,* **1 g**$^+$) or the *ortho*-iodobromo compounds (*i.e.,* **1i**$^+$), which suggests that in the context of organohalides, the large atomic radius and high polarizability of iodine may be critical to the observed X−X interactions; potential translation of X−X interaction to the smaller halogens such as in hypervalent bromine chemistry remains an area for development.[40,41] In contrast, a BCP is observed for the iodanyl radical cation derived from **1j** (the BCP is observed both for **1j**$^+$ and the corresponding deprotonated analogue, see Figure S18). This result is consistent with previous reports that an *ortho*-carboxylate substituent can stabilize iodanyl radicals generated during the reduction of I(III) compounds.[24,25]

Isolation of **1a**$^+$ provided the first opportunity to directly evaluate the reactivity of organic I(II) derivatives in substrate functionalization. Treatment of **1a**$^+$ reactions with biarylamide **2** and [TMA]OAc in hfip resulted in the immediate disappearance of the blue color and the evolution of carbazole **3** (35% yield) and quantitative recovery of **1a** (Figure 6a). With demonstration of the chemical competence of iodanyl radical **1a**$^+$ in substrate functionalization and the significantly decreased oxidation potential of **1a** as compared to **1b**, we

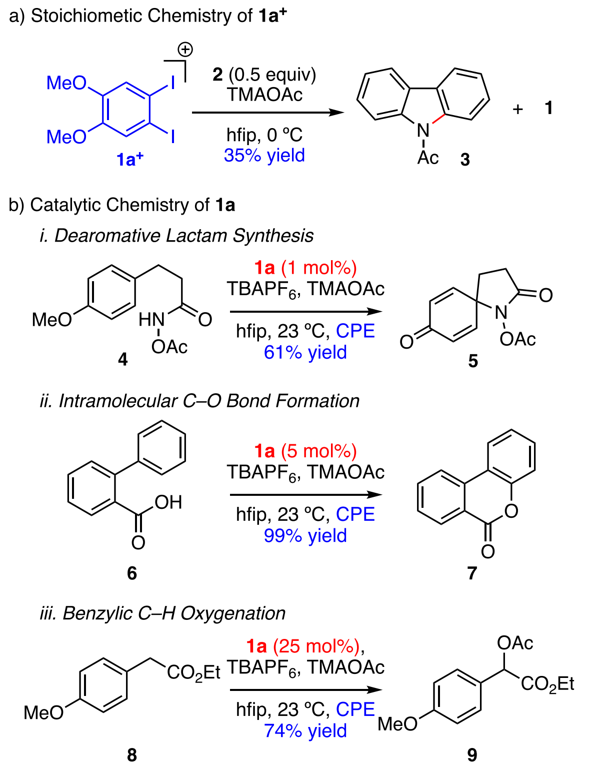

Figure 6. (a) Iodanyl radical promotes conversion of **2** to **3**. (b) Diiodide **1** catalyzes (i) oxidative dearomatization, (ii) lactone cyclization, and (iii) benzylic acetoxylation. CPE at 1.22 V vs Fc$^+$/Fc. Reactions were optimized to the lowest catalyst loading without the current density suffering (>1.0 mA).

examined the potential to achieve other C−E bond-forming reactions (Figure 6b). Oxidative dearomatization of **4** was successfully demonstrated with a catalyst loading as low as 1 mol % producing 61% yield of product **5**. C(sp^2)−O bond formation can be accomplished from biarylcarboxylic acid **6** to afford **7** under electrocatalytic condition (5 mol % **1a**) loading.[42] In the absence of **1a**, no background oxidation of either **4** or **6** was observed. Additionally, intermolecular benzylic acetoxylation of **8** to generate **9** was accomplished in 74% although higher catalyst loading (25 mol %) was required for high yield. Direct oxidation of **8** for extended reaction times in the absence of catalysts shows greater preference for the benzylic ketone product (40%) and only 20% acetoxylated product **9**.

■ CONCLUSIONS

In conclusion, here, we introduce a new aryl iodide electrocatalyst—1,2-diiodo-4,5-dimethoxybenzene (**1a**)—that operates at catalyst loadings down to 0.5 mol %. This catalyst activity is ascribed to a combination of reversible veratrole-based electrochemistry and cooperative I−I bonding that stabilizes the iodanyl radical intermediate that results from one-electron oxidation. Isolation of the incipient iodanyl radical enabled both complete characterization of the first formally I(II)-based organic molecule and direct interrogation of the substrate functionalization chemistry of this exotic species in substrate functionalization reactions. The results described here (1) suggest that I(II) intermediates can be catalytically competent rather than simply intermediates *en route* to more traditionally invoked I(III) species and (2)

https://doi.org/10.1021/jacs.2c05562
J. Am. Chem. Soc. 2022, 144, 13913−13919

expand the reactivity modes that are available to iodine-based catalysts in metal-free substrate oxidation chemistry.

■ ASSOCIATED CONTENT

Supporting Information

The Supporting Information is available free of charge at https://pubs.acs.org/doi/10.1021/jacs.2c05562.

Experimental procedures, analytical data, X-ray crystallographic analysis of compound **1a**$^+$, DFT calculation details, ^{1}H NMR spectra for all compounds, and ^{13}C NMR data for newly synthesized compound **19** (PDF)

Accession Codes

CCDC 2173759–2173760 contain the supplementary crystallographic data for this paper. These data can be obtained free of charge via www.ccdc.cam.ac.uk/data_request/cif, or by emailing data_request@ccdc.cam.ac.uk, or by contacting The Cambridge Crystallographic Data Centre, 12 Union Road, Cambridge CB2 1EZ, UK; fax: +44 1223 336033.

■ AUTHOR INFORMATION

Corresponding Author

David C. Powers – *Department of Chemistry, Texas A&M University, College Station, Texas 77843, United States;* orcid.org/0000-0003-3717-2001; Email: powers@chem.tamu.edu

Authors

Brandon L. Frey – *Department of Chemistry, Texas A&M University, College Station, Texas 77843, United States*

Matthew T. Figgins – *Department of Chemistry, Texas A&M University, College Station, Texas 77843, United States*

Gerard P. Van Trieste, III – *Department of Chemistry, Texas A&M University, College Station, Texas 77843, United States*

Raanan Carmieli – *Department of Chemical Research Support, Weizmann Institute of Science, Rehovot 76100, Israel;* orcid.org/0000-0003-4418-916X

Complete contact information is available at: https://pubs.acs.org/10.1021/jacs.2c05562

Author Contributions

The manuscript was written through contributions of all authors.

Notes

The authors declare no competing financial interest.

■ ACKNOWLEDGMENTS

The authors acknowledge the National Institutes of Health (R35GM138114) and the Welch Foundation (A-1907) for support. Exploratory studies of the electrochemistry of **1a** were supported by the National Science Foundation (CAREER 1848135). Structure determinations were collected at NSF's ChemMatCARS Sector 15, which is principally supported by the Divisions of Chemistry (CHE) and Materials Research (DMR), NSF, under Grant NSF/CHE-1834750. Use of the Advanced Photon Source, an Office of Science User Facility operated for the U.S. DOE Office of Science by Argonne National Laboratory, was supported by the U.S. DOE under Contract DE-AC02-06CH11357. The computational work was completed with resources provided by the Texas A&M University High Performance Research Computing (HPRC) center.

■ REFERENCES

(1) Francke, R.; Little, R. D. Redox catalysis in organic electrosynthesis: basic principles and recent developments. *Chem. Soc. Rev.* **2014**, *43*, 2492–2521.

(2) Yan, M.; Kawamata, Y.; Baran, P. S. Synthetic Organic Electrochemical Methods Since 2000: On the Verge of a Renaissance. *Chem. Rev.* **2017**, *117*, 13230–13319.

(3) Brand, J. P.; González, D. F.; Nicolai, S.; Waser, J. Benziodoxole-based hypervalent iodine reagents for atom-transfer reactions. *Chem. Commun.* **2011**, *47*, 102–115.

(4) Charpentier, J.; Früh, N.; Togni, A. Electrophilic Trifluoromethylation by Use of Hypervalent Iodine Reagents. *Chem. Rev.* **2015**, *115*, 650–682.

(5) Sousa, E. S. F. C.; Tierno, A. F.; Wengryniuk, S. E. Hypervalent Iodine Reagents in High Valent Transition Metal Chemistry. *Molecules* **2017**, *22*, 780–834.

(6) Yoshimura, A.; Yusubov, M. S.; Zhdankin, V. V. Synthetic applications of pseudocyclic hypervalent iodine compounds. *Org. Biomol. Chem.* **2016**, *14*, 4771–4781.

(7) Yoshimura, A.; Zhdankin, V. V. Advances in Synthetic Applications of Hypervalent Iodine Compounds. *Chem. Rev.* **2016**, *116*, 3328–3435.

(8) Aertker, K.; Rama, R. J.; Opalach, J.; Muñiz, K. Vicinal Difunctionalization of Alkenes under Iodine(III) Catalysis involving Lewis Base Adducts. *Adv. Synth. Catal.* **2017**, *359*, 1290–1294.

(9) Fuchigami, T.; Fujita, T. Electrolytic Partial Fluorination of Organic Compounds. 14. The First Electrosynthesis of Hypervalent Iodobenzene Difluoride Derivatives and Its Application to Indirect Anodic gem-Difluorination. *J. Org. Chem* **1994**, *59*, 7190–7192.

(10) Kong, X.; Lin, L.; Chen, X.; Chen, Y.; Wang, W.; Xu, B. Electrochemical Oxidative Syntheses of NH-Sulfoximines, NH-Sulfonimidamides and Dibenzothiazines via Anodically Generated Hypervalent Iodine Intermediates. *ChemSusChem* **2021**, *14*, 3277–3282.

(11) Maity, A.; Frey, B. L.; Hoskinson, N. D.; Powers, D. C. Electrocatalytic C–N Coupling via Anodically Generated Hypervalent Iodine Intermediates. *J. Am. Chem. Soc.* **2020**, *142*, 4990–4995.

(12) Massignan, L.; Tan, X.; Meyer, T. H.; Kuniyil, R.; Messinis, A. M.; Ackermann, L. C–H Oxygenation Reactions Enabled by Dual Catalysis with Electrogenerated Hypervalent Iodine Species and Ruthenium Complexes. *Angew. Chem., Int. Ed.* **2020**, *59*, 3184–3189.

(13) Wirth, T. Iodine(III) mediators in electrochemical batch and flow reactions. *Curr. Opin. Electrochem.* **2021**, *28*, 100701.

(14) Francke, R. Recent progress in the electrochemistry of hypervalent iodine compounds. *Curr. Opin. Electrochem.* **2021**, *28*, 100719.

(15) Banks, D. F.; Huyser, E. S.; Kleinberg, J. Free-Radical Reactions of Iodobenzene Dichloride with Hydrocarbons. *J. Org. Chem* **1964**, *29*, 3692–3693.

(16) Bloomfield, G. F. 43. Rubber, polyisoprenes, and allied compounds. Part VI. The mechanism of halogen-substitution reactions, and the additive halogenation of rubber and of dihydromyrcene. *J. Chem. Soc.* **1944**, 114–120.

(17) Tanner, D. D.; Van Bostelen, P. B. Free-radical chlorination reactions of iodobenzene dichloride. *J. Org. Chem* **1967**, *32*, 1517–1521.

(18) Wang, X.; Studer, A. Iodine(III) Reagents in Radical Chemistry. *Acc. Chem. Res.* **2017**, *50*, 1712–1724.

(19) Hyun, S.-M.; Yuan, M.; Maity, A.; Gutierrez, O.; Powers, D. C. The Role of Iodanyl Radicals as Critical Chain Carriers in Aerobic Hypervalent Iodine Chemistry. *Chem* **2019**, *5*, 2388–2404.

(20) Habert, L.; Cariou, K. Photoinduced Aerobic Iodoarene-Catalyzed Spirocyclization of N-Oxy-amides to N-Fused Spirolactams. *Angew. Chem., Int. Ed.* **2021**, *60*, 171–175.

(21) Huang, J.; Pan, B.; Duan, W.; Wei, X.; Assary, R. S.; Su, L.; Brushett, F. R.; Cheng, L.; Liao, C.; Ferrandon, M. S.; Wang, W.; Zhang, Z.; Burrell, A. K.; Curtiss, L. A.; Shkrob, I. A.; Moore, J. S.; Zhang, L. The lightest organic radical cation for charge storage in redox flow batteries. *Sci. Rep.* **2016**, *6*, 32102–32111.

(22) Sagl, D. J.; Martin, J. C. The stable singlet ground state dication of hexaiodobenzene: possibly a sigma-delocalized dication. *J. Am. Chem. Soc.* **1988**, *110*, 5827−5833.
(23) Gallardo-Donaire, J.; Martin, R. Cu-Catalyzed Mild C(sp2)−H Functionalization Assisted by Carboxylic Acids en Route to Hydroxylated Arenes. *J. Am. Chem. Soc.* **2013**, *135*, 9350−9353.
(24) Amey, R. L.; Martin, J. C. Synthesis and reaction of substituted arylalkoxyiodinanes: formation of stable bromoarylalkoxy and aryldialkoxy heterocyclic derivatives of tricoordinate organoiodine-(III). *J. Org. Chem* **1979**, *44*, 1779−1784.
(25) Amey, R. L.; Martin, J. C. Identity of the chain-carrying species in halogenations with bromo- and chloroarylalkoxyiodinanes: selectivities of iodinanyl radicals. *J. Am. Chem. Soc.* **1979**, *101*, 3060−3065.
(26) Sandford, C.; Edwards, M. A.; Klunder, K. J.; Hickey, D. P.; Li, M.; Barman, K.; Sigman, M. S.; White, H. S.; Minteer, S. D. A synthetic chemist's guide to electroanalytical tools for studying reaction mechanisms. *Chem. Sci.* **2019**, *10*, 6404−6422.
(27) Costentin, C.; Savéant, J.-M. Multielectron, Multistep Molecular Catalysis of Electrochemical Reactions: Benchmarking of Homogeneous Catalysts. *ChemElectroChem* **2014**, *1*, 1226−1236.
(28) The significant deviation from an ideally reversible system prevents traditional electroanalytical analysis of 1a via the Randles-Sevcik equation making direct calculation of the number of electrons transferred unreliable.
(29) Horibe, T.; Ohmura, S.; Ishihara, K. Structure and Reactivity of Aromatic Radical Cations Generated by FeCl3. *J. Am. Chem. Soc.* **2019**, *141*, 1877−1881.
(30) Rathore, R.; Wadumethrige, S. H. Highly robust cation radical salts: Aromatic oxidants from cycloannulated aromatic donors. *J. Photochem. Photobiol., A.* **2019**, *382*, 111882−111893.
(31) All optimizations were performed at the B3LYP-D3BJ/BS1 (BS1 defined in the Computational Methods Details in the SI) level of theory. TD−DFT single points were performed on the optimized geometries to calculate the first 30 excitations.
(32) Toybenshlak, M.; Carmieli, R. A New and Robust Method for In-situ EPR Electrochemistry. *Isr. J. Chem.* **2019**, *59*, 1020−1026.
(33) Kita, Y.; Tohma, H.; Hatanaka, K.; Takada, T.; Fujita, S.; Mitoh, S.; Sakurai, H.; Oka, S. Hypervalent Iodine-Induced Nucleophilic Substitution of para-Substituted Phenol Ethers. Generation of Cation Radicals as Reactive Intermediates. *J. Am. Chem. Soc.* **1994**, *116*, 3684−3691.
(34) Dohi, T.; Ito, M.; Yamaoka, N.; Morimoto, K.; Fujioka, H.; Kita, Y. Hypervalent iodine(III): selective and efficient single-electron-transfer (SET) oxidizing agent. *Tetrahedron* **2009**, *65*, 10797−10815.
(35) Other one electron oxidants including Fe(III), Ce(IV), and nitrosium salts produced indistinguishable UV-vis spectra upon oxidation of **1a** however were unsuccessful in producing single crystals.
(36) Yang, W.; Zhang, L.; Xiao, D.; Feng, R.; Wang, W.; Pan, S.; Zhao, Y.; Zhao, L.; Frenking, G.; Wang, X. A diradical based on odd-electron σ-bonds. *Nat. Commun.* **2020**, *11*, 3441−3449.
(37) Zhang, S.; Wang, X.; Su, Y.; Qiu, Y.; Zhang, Z.; Wang, X. Isolation and reversible dimerization of a selenium−selenium three-electron σ-bond. *Nat. Commun.* **2014**, *5*, 4127−4134.
(38) Zhang, S.; Wang, X.; Sui, Y.; Wang, X. Odd-Electron-Bonded Sulfur Radical Cations: X-ray Structural Evidence of a Sulfur−Sulfur Three-Electron σ-Bond. *J. Am. Chem. Soc.* **2014**, *136*, 14666−14669.
(39) Bartashevich, E. V.; Yushina, I. D.; Stash, A. I.; Tsirelson, V. G. Halogen Bonding and Other Iodine Interactions in Crystals of Dihydrothiazolo(oxazino)quinolinium Oligoiodides from the Electron-Density Viewpoint. *Cryst. Growth Des.* **2014**, *14*, 5674−5684.
(40) Mohebbati, N.; Sokolovs, I.; Woite, P.; Lõkov, M.; Parman, E.; Ugandi, M.; Leito, I.; Roemelt, M.; Suna, E.; Francke, R. Electrochemistry and Reactivity of Chelation-stabilized Hypervalent Bromine(III) Compounds. *Chem. − Eur. J.* **2022**, No. e202200974.
(41) Sokolovs, I.; Mohebbati, N.; Francke, R.; Suna, E. Electrochemical Generation of Hypervalent Bromine(III) Compounds. *Angew. Chem., Int. Ed.* **2021**, *60*, 15832−15837.
(42) Togo, H.; Muraki, T.; Yokoyama, M. Remote functionalization (1): Synthesis of γ- and δ-lactones from aromatic carboxylic acids. *Tetrahedron Lett.* **1995**, *36*, 7089−7092.

https://doi.org/10.1021/jacs.2c05562
J. Am. Chem. Soc. 2022, 144, 13913−13919